Structural Properties of Early-Type Galaxies from the SDSS DR2 [*]

Feng-Shan Liu[1,2,3], Zu-Gan Deng[2], Hong Wu[1] and Xiao-Yang Xia[3]

[1] National Astronomical Observatories, Chinese Academy of Sciences, Beijing 100012, China; *lfs@bao.ac.cn*
[2] Graduate School of Chinese Academy of Sciences, Beijing 100049, China
[3] Department of Physics, Tianjin Normal University, Tianjin 300074, China

Abstract Two-dimensional bulge/disk light decomposition with GIM2D in both the r- and g-bands has been applied to a sample of 129 early-type galaxies brighter than 13.5 magnitude in the r-band, selected from the Sloan Digital Sky Survey Data Release 2. Intensity-weighted Fourier coefficient $\langle a_4/a \rangle$ was also derived for each sample galaxy. Our analysis shows that there are correlations between bulge-to-total light ratio (B/T) with bulge Sérsic index n_B and between bulge and disk scale sizes. Isophotal shape parameter $\langle a_4/a \rangle$ is not correlated with B/T and n_B. Both bulge and disk components satisfy a color-magnitude relation. The κ space Fundamental Plane analysis shows that galaxies with larger B/T tend to lie tighter and closer to the line of $\kappa_1 + \kappa_2 = 8$ (the so-called "zone of avoidance") than the galaxies with smaller B/T. It indicates that existence of the disk component may lead to scatter of the distribution on the Fundamental Plane. Our analysis also shows that $\kappa_1 + \kappa_2$ correlates with $(g\text{-}r)$ color and B/T, but does not correlate with $\langle a_4/a \rangle$ for early-type galaxies. The fitted parameters and other retrieved parameters used in this paper for all sample galaxies are available online.

Key words: galaxies: elliptical and lenticular, cD — galaxies; photometry — galaxies; structure — galaxies

1 INTRODUCTION

The morphology and structure of galaxies carry important information on the history of their formation and evolution. The two most prominent components of a galaxy are its bulge and disk. They have quite different dynamical properties and are considered to have followed different paths of formation. For a period after Hubble (1936) introduced his morphological classification of galaxies, the elliptical (E) galaxies were thought to be the simplest stellar systems without a disk or internal structure. There is a population of galaxies called lenticular (S0) galaxies, which is the transition type between elliptical galaxies and disk galaxies, with a similar stellar population and photometric and dynamical properties to the elliptical galaxies (e.g., Djorgovski & Davis 1987; Dressler 1987; Visvanathan & Sandage 1977; Lugger 1984; Jørgensen, Franx &Kjærgaard 1996; Terlevich et al. 1999; Bender et al. 1988,1989; Hao et al. 2006; Cool et al. 2006). The elliptical and lenticular galaxies are ususally combined into one class, called the early-type galaxies. As the observations with higher resolution and sensitivity become available, it has been revealed that even elliptical galaxies have a wealth of internal structures. Embedded faint disks do exist in many E galaxies (e.g., Carter 1987; Capaccioli 1987; Bender et al. 1989; Rix & White 1990). Later observations have confirmed that a large proportion of elliptical galaxies do host embedded disk components. Some authors suggested

that 1/3 to 2/3 ellipticals (e.g., Davies 2000) or even all ellipticals may have disks, but they are too faint to be detected (Burstein et al. 2001).

Previous studies showed that there may be two types of stellar disks embedded in early-type galaxies and they differ in size (e.g., Davies 2000; McDermid et al. 2006). The smaller ones usually have scale sizes less than about a hundred pc and are made up of a younger stellar population, while the larger ones usually have scale sizes of $\geq$ kpc and most of them have a stellar population indistinguishable from the spheroid components of galaxies. The discovery of embedded disks in early-type galaxies poses problems on their formation, on the formation of the early-type galaxies, and on the origin of Hubble sequence of galaxies (e.g., Kormendy 1984; Balcells & Quinn 1990; Hernquist & Barnes 1991; Weil & Hernquist 1993).

Several methods have been developed to probe the structures of early-type galaxies, among which the one-dimensional (1-D) or two-dimensional (2-D) bulge/disk light decomposition (Kent 1985; Iodice et al. 1999; de Jong et al. 2004) and isophotal shape analysis (e.g., Lauer 1985; Bender et al. 1988,1989; Hao et al. 2006) have been popular. In the early research, bulge/disk light decomposition was usually carried out with a classical de Vaucouleurs' (1948) $R^{1/4}$-law profile bulge plus an exponential profile disk (e.g., Kent 1985; Jørgensen & Franx 1994; Saglia et al. 1997). Recently, such decompositions are often substituted by a generalization of the $R^{1/4}-$law (Sérsic 1968) by generalizing the 1/4 to $1/n$. In generalized scheme, the exponential and $R^{1/4}-$ laws correspond to $n =$1 and 4, respectively. The Sérsic profile would account for part of the observed deviation from the $R^{1/4}-$law for the bulges of galaxies (Caon, Capaccioli & D'Onofrioo 1993; Graham & Colless 1997; de Jong et al. 2004). With the 2-D bulge/disk light decompositions, de Jong et al. (2004) analysed the structural properties of 558 early-type galaxies in the EFAR sample and checked the relations among structural parameters. Tasca & White (2005) estimated the contribution of the bulges and disks to the local luminosities for a sample of about 1800 early-type galaxies selected from SDSS in both r- and i-bands. They also have made a correction of systematic errors caused by the finite thickness of the disks. However, how can we confirm that the detected exponential components in the two-component decompositions of the early-type galaxies are really connected to the disks existing in the galaxies? One possibility is to check whether these disks are rotationally supported as are disks in spiral galaxies, with the aid of kinematical measurement. However, stellar kinematical measurement for a large enough sample of galaxies requires a prohibitive amount of telescope time. A large project such as SAURON (Bacon et al. 2001; Emsellem et al. 2004), which after making great efforts have only obtained results for 48 early-type galaxies so far. Moreover, owing to the techincal limitations, these measurements are usually restricted to the inner regions of the galaxies.

In this work, we attempt to explore this question in a different way. We shall examine whether the detected components by 2-D bulge/disk light decomposition satisfy certain global properties such as the well-known color-magnitude relation (CMR), and how these scaling relations of early-type galaxies such as the Fundamental Plane (FP) depend on the bulge-to-total light ratio obtained from the decomposition. We shall also compare in our analysis some SAURON early-type galaxies with kinematical measurements. We selected 129 nearby E/S0 galaxies brighter than r magnitude 13.5 from Sloan Digital Sky Survey (SDSS) Data Release 2 (DR2) as our sample for studying their structural properties and scaling relations (CMR and FP). We shall also investigate the relations between the parameters obtained from the 2-D bulge/disk light decomposition and the isophotal shape parameters. Two-Dimensional bulge/disk light decomposition in both Sloan g- and r-bands have been carried out. Our analysis provides evidence that the bulge and disk components determined from the 2-D light decomposition have the expected global properties in a statistical sense.

This paper is organized as follows. The sample selection is described in Section 2. Preliminary data reduction and a brief introduction on 2-D bulge/disk light decomposition and Fourier expansion are given in Section 3. The results and analysis are presented in Section 4. A summary and a discussion are presented in Section 5. Throughout this paper we use a cosmology of $\Omega_m = 0.3, \Omega_\Lambda = 0.7$ and $H_0 = 70\,\mathrm{km\,s^{-1}\,Mpc^{-1}}$.

2 THE SAMPLE

Our analysis is based on a sample of nearby bright early-type galaxies selected from SDSS DR2. First, we picked out 1067 galaxies brighter than $13.5\,\mathrm{mag}$ (model magnitude) in the Sloan r-band. Then, galaxies which have late-type and peculiar morphologies were removed from the sample. We also excluded galaxies which are contaminated by companion objects or with visible substructures (as dusty feature, rings, or bars,
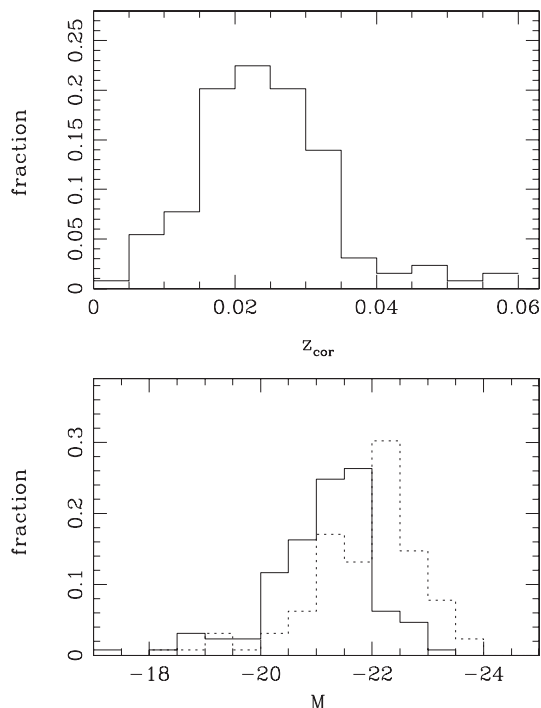
Fig. 1 Number distributions of the corrected redshifts (top panel) and of the extinction-corrected absolute magnitudes (bottom panel) in our sample. In the bottom panel, solid line stands for the g-band, dotted line for the r-band.

etc.) by carefully examining their images in all five bands. Galaxies with saturated images or located at the edge of the corrected frame (Stoughton et al. 2002) are also excluded. This resulted in 237 galaxies with relatively smooth images. An additional requirement is that galaxies in the sample should have velocity dispersion data available from the SDSS spectra. In total, we constructed a sample of 131 early-type galaxies from the 237 galaxies, and it should be approximately a flux limited sample. The main goal with above selection criteria is to ensure that all the selected galaxies are apparently bright, large and smooth to guarantee a high quality photometry. Our sample does not include nearly edge-on S0 galaxies since such galaxies are difficult to be discriminated S0 from spiral galaxies and usually with distinct dusty feature. We calculated the luminosity and angular diameter distances of each source with the Local Group relative redshifts given in Blanton et al. (2005). There are two objects with negative redshifts, these were excluded from the following analysis. So, the final sample includes 129 bright early-type galaxies. The corrected redshift number distribution of the 129 galaxies is shown in the top panel of Figure 1. Beause the images in u- and z-bands are relatively shallow, and the i-band images suffer from the 'red halo' effect (Michard 2002; Wu et al. 2005), the results of their image decomposition would be affected, so our analysis was based on only the images in the g-and r- bands. The $(2048 \times 1489$ pixels) imaging frames of all targets in the sample were extracted from DR2 archive. More information on the SDSS DR2 can be found in Abazajian et al. (2004). In the bottom panel of Figure 1, we present the number distributions of our observed absolute magnitudes in the two bands, to $\mu = 25\,\mathrm{mag\,arcsec}^{-2}$ in the g-band after correction for the Galactic extinction. The redshifts being low, no k-correction was applied.

3 DATA REDUCTION

3.1 Preliminary Data Reduction

The corrected frames obtained from SDSS have been processed by the photometric pipeline (PHOTO) with bias-subtraction, flat-field correction, and corrections for cosmic rays and pixel defects. The astromet-
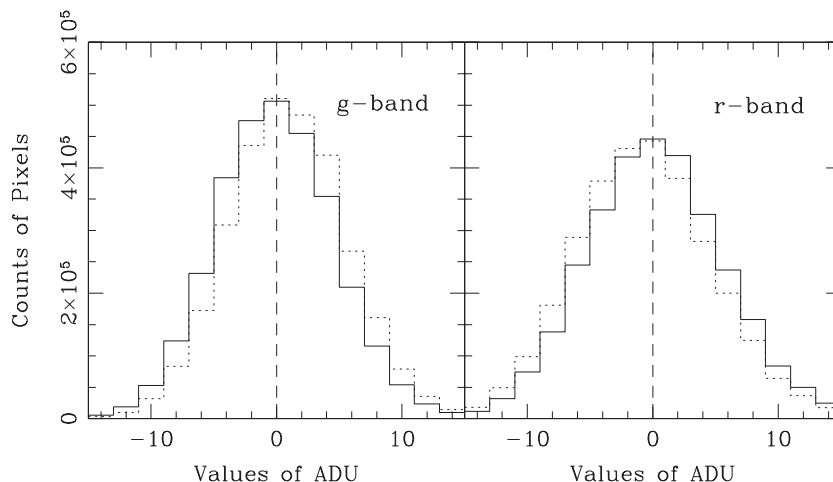
Fig. 2 Comparison of flux distributions in frames with background subtraction by SEXTRACTOR (dotted histogram) and by our method (solid histsogram). The data refer to the frames containg the target galaxy UGC 07177 in the g-band (left panel) and the r-band (right panel).

ric solutions for the five bands are obtained from the astrometric pipeline (ASTROM), with typical errors well blow $0.1''$ (Stoughton et al. 2002). However, as noticed by Wu et al. (2005), structures still exist in many frames, which might be due to bias in the CCDs. For galaxies which happen to be located on such structures, both the background subtraction and the fitting of the light at the outer part of the image of low surface brightness, can be significantly affected. So we applied the corrections given by Wu et al. (2005). To obtain the real brightness of the target objects, an accurate sky background subtraction is crucial. In previous works, one usually subtracted a flat background or a sky background obtained by the SEXTRACTOR (Bertin & Arnouts 1996) photometry package (Tasca & White 2005). However, sky background in the SDSS frames is usually twisty and varies along different directions. To obtain a better sky background, we mask all objects in the frame by SEXTRACTOR to generate a background-only image, and then fit both the rows and columns of the background image separately with a second order legendre function. Since most of the sample galaxies have sizes of only a few arcminutes and are small comparing with the size of the frame, it is easy to isolate sufficeint sky regions to fit a reasonable sky background. A representative example for comparing the quality of background-subtraction by these two methods is given in Figure 2. The target object here is UGC 07177. The result obtained with SEXTRACTOR is shown by the dotted line and the one by our method, by the solid line. The g-band results are in the left panel, the r-band results, in the right. It is clear that solid line histogram (from our method) is nearly symmetrical and with a nearly zero mean, indicating a good sky background subtraction, while the dotted-line histogram (obtained with SEXTRACTOR) is of a relatively inferior quality. So we subtracted the sky background with our method mentioned above from the corrected frames and obtained the "background-free" frames.

3.2 Two-Dimensional Bulge/Disk Light Decomposition

The best-fitted PSF-convolved 2-D bulge plus disk model for each galaxy in the sample has been found with the publicly available GIM2D (Simard et al. 2002) package, which has been well-tested on different galaxy samples (Marleau & Simard 1998; de Jong et al. 2004; Tasca & White 2005). Here, we give a brief outline of the GIM2D package. Readers who like to know more details can refer to Simard et al. (2002) and GIM2D Home Page [1]. Here, an early-type galaxy is assumed to be composed of two components: a disk with exponential profile

$$\mu(r) = \mu_0 e^{-r/h},$$

---

[1] *http://www.hia-iha.nrc-cnrc.gc.ca/STAFF/lsd/gim2d/*

where μ_0 is the central surface brightness of the disk, h is the disk scale length, and a bulge described by a Sérsic profile,

$$\mu(r) = \mu_{\mathrm{e}} e^{-b[(r/r_{\mathrm{e}})^{1/n}-1]},$$

where $\mu(r)$ is the surface brightness at r along the semi-major axis, and μ_{e} is the effective surface brightness, defined as the surface brightness at the effective semi-major axis radius r_{e}, defined as the projected radius enclosing half of the light in this component (Capaccioli 1989). The parameter b depends on the Sérsic index n and is set to be $1.9992n - 0.3271$ (Sérsic 1968), The de Vaucouleurs profile corresponds to $n = 4$, and the expobential profile, to $n = 1$. Values of n greater than 4 are found in some bright large galaxies (Iodice et al. 1999). For clarity, we shall use from now on, the subscripts 'B', 'D', and 'T' to refer to the bulge, disk, and the whole galaxy, respectively. We denote the semi-major axis effective radius with subscript 'e' (r_{e}) and the equivalent radius with subscript '0' (r_0), thus, $r_0 = r_{\mathrm{e}}\sqrt{1 - \epsilon}$.

The de Vaucouleurs profile ($n = 4$) has been extensively used to describe the light profiles of bulges of early-type galaxies, though it has been found that, for some bulges, the profile deviates from the $R^{1/4}$-law (Binney & Merrifield 1998). To compare the fitted results with the de Vaucouleurs and Sérsic bulge profiles, we made both fittings. More detailed comparisons can be found in Allen et al. (2006).

The GIM2D package has a maximum of 12 fitting parameters: The total flux F_{total} from the model integrated to $r = \infty$; the bulge-to-total light ratio (B/T), defined as $F_{\mathrm{bulge}}/F_{\mathrm{total}}$; the semi-major axis effective radius of the bulge $r_{e,B}$; the bulge ellipticity ε_B, defined as $\varepsilon_B \equiv 1 - b_B/a_B$, where a_B and b_B are the bulge semi-major and semi-minor axes respectively; the bulge position angle ϕ_B; the scale length of the disk h; the inclination of the disk i ($i = 0$ for face-on); the disk position angle ϕ_D; the subpixel dx and dy offsets of the galaxy's center; the residual background level db; and the Sérsic index n_B of the bulge. One or more of the parameters can be frozen at their initial values, if necessary, depending on the particular scientific goal on hand. The best-fit parameters and their confidence intervals are determined with the Metropolis algorithm (Metropolis et al. 1953; Saha & Williams 1994), which uses the χ^2 test to determine the region of maximum likelihood in the multi-parameter space. Before doing 2-D decomposition of the sample galaxies, we follow the procedure of de Jong et al. (2004) to test the GIM2D package with 600 artificial galaxies with characteristics similar to real Sloan g-band data. The images were of size 1000×1000 pixels and the pixel size was $0.396''$. Galaxy images were created in a Monte-Carlo fashion with total magnitudes sampled uniformly between g-band apparent magnitudes 12 and 14.5, the B/T ratio was sampled uniformly between 0.05 and 1.0, bulges with $18 \leq \mu_{e,B} \leq 24$ and $1 \leq n_B \leq 9$, and disks with $19 \leq \mu_{0,D} \leq 24$, and $0.1 \leq \cos(i) \leq 1.0$. The CCD read noise, gain and sky background were set comparable to most of the SDSS observations, and Poisson noise was added appropriate for the detected flux level. The galaxies were convolved by a typical PSF function from SDSS. We use the Sérsic bulge plus exponential disk model to fit the artificial galaxies following the same procedure as for real galaxies. Our results show that the parameters of the total galaxy and the disk can be recovered to within $5\% - 15\%$ of the set values, and the bulge parameters can be recovered to within $20\% - 30\%$: these results are similar to those obtained by de Jong et al. (2004) for the EFAR galaxies. This test confirms that GIM2D can be reasonably well used to perform 2-D light decomposition of the SDSS data in statistical studies.

We apply the SEXTRACTOR package to determine the detection threshold and define the isophotal area where the image signal is above the detection threshold. We have chosen a threshold 1.5 times the background noise, which is on average equal to ~ 25 mag arcsec^{-2} in the g-band. Then, we apply SEXTRACTOR to extract two stamp images centered on the target and about 10 times larger than the area of the isophote defined by the SEXTRACTOR. The first stamp image is cut from the corrected background-free frame, while the second contains the corresponding pixels on which the object, background and contamination objects are marked with different flags. The seeing of SDSS is about 1.5 arcsec, so structures smaller than that can not be resolved. On the other hand, the center of a galaxy is rather complex and it is difficult to use the simple model to give a good fit. We therefore mask the central seeing-size region in the stamp image (de Jong et al. 2004), i.e., our analysis is focused on objects with rather large disks. We used all 12 parameters to fit each sample galaxy. The model image produced with the parameters is convolved with a PSF before comparing with the real data. A simple Gaussian was usually used in the convolution before. Trujillo et al. (2001) studied the effects of seeing on the parameters of the Sérsic profile analytically using a Gaussian PSF, which showed that the effects of seeing are not negligible (see Young & Currie 2001 and reference
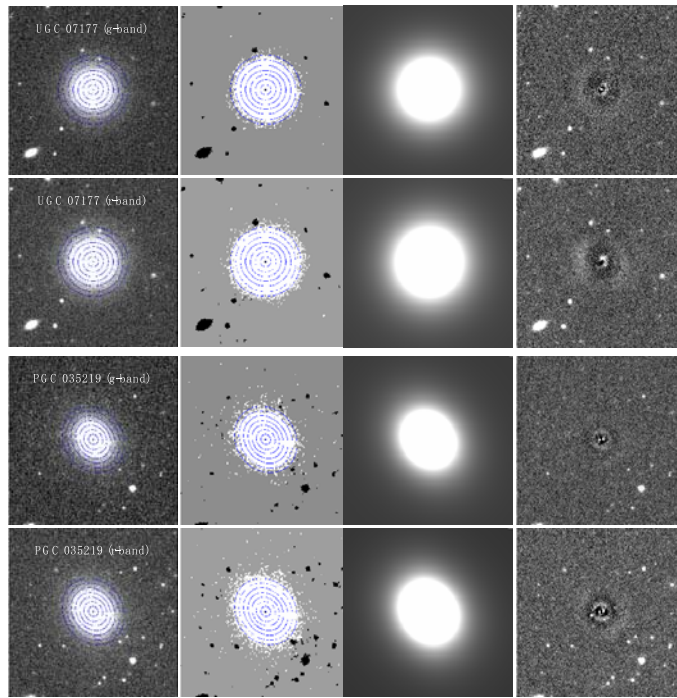
Fig. 3 Examples of the sky background-free stamp images, the contamination masked images, the best model ("$r^{1/n}$ + exp") images, and the residual images (from left to right) for UGC 07177 (in first and second lines) and PGC 035219 (in third and fourth lines) respectively in the Sloan g-band and r-band given in the left most images. The outermost annuli are where the local surface brightness in the g-band is $\mu = 25$ mag arcsec^{-2}.

therein). However, the PSF of real observation is not exactly Gaussian (Fried 1996; Woolf 1982). For the SDSS frames, Stoughton et al. (2002) pointed out that the PSF FWHM can vary up to 15% from one side to another, even in the absence of atmospheric inhomogeneity. So, the real effects of it on the fitted parameters are difficult to estimate. Therefore, it is better to use realistic PSFs. We used the method [2] provided by the SDSS to construct a realistic PSF model for each sample galaxy at the proper position in the frame. The GIM2D package provides 99% confidence limits on the fitted parameters, based on the topology of the parameter space that is built up during the fitting process, which takes the uncertainties in the fitted parameters into account. In this work we only give these errors. Small uncertainties involving the sky level and seeing are not included since we can make a better sky background subtraction and apply realistic PSFs.

Representative examples of the fitting are given for two objects, UGC 07177 and PGC 035219. See Figure 3. From left to right, are displayed the background-free stamp images centered on the targets, the stamp images with contamination flagged, the best fitted model ("$r^{1/n}$ +exp") images, and the corresponding residual images in the g- and r-bands, respectively.

Figure 4 compares the fitted radial profiles and observed profiles for these two galaxies. For UGC 07177, we show the results from both fittings, with the "$r^{1/4}$ + exp" (a and b) and "$r^{1/n}$ + exp" (c and d) models, because its bulge profile deviated from the $R^{1/4}$-law. For PGC 035219, its profile is close to the $R^{1/4}$-law, so we do not show the result the "$r^{1/4}$ + exp" model fitting. It can be seen from the comparisons, that the bulges of some early-type galaxies do have their profiles deviating from the de Vaucouleurs law, and for these, the "$r^{1/4}$ + exp" model can not give a fitting as good as the "$r^{1/n}$ +exp" model. We can also see that the fitted profiles in the two bands are somewhat different, which may be due to the existence of color gradients in early-type galaxies.

---

[2] For details please see *http://www.sdss.org/dr3/products/images/read_psf.html*
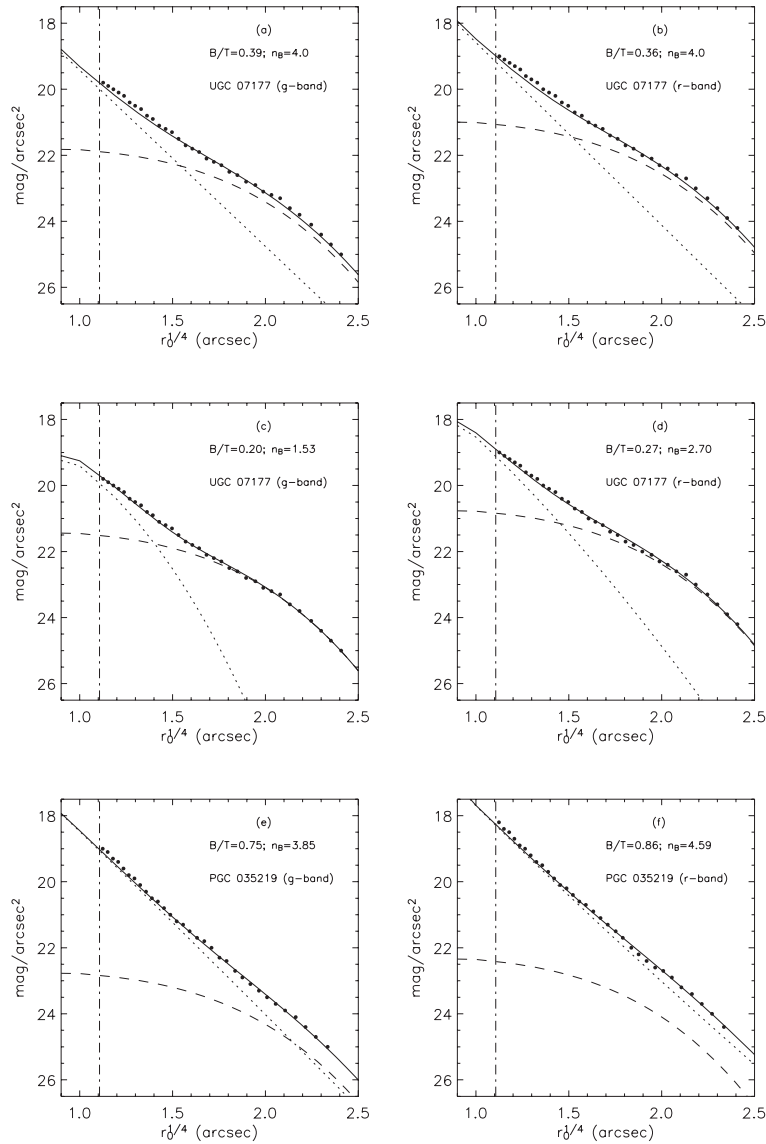
Fig. 4 Comparison between the observed and best fitted radial profiles. From top to bottom, the best fitted profiles of UGC 07177 with the "$r^{1/4} + \exp$" model, with the "$r^{1/n} + \exp$" model, and the best fitted profile of PGC 035219 with the "$r^{1/n} + \exp$" model. Left panels are for the g- band, and right for the r-band. Solid lines are for the whole galaxy, dotted lines for the bulge, dashed lines for the disk, vertical dot-dashed lines the seeing region, and solid dots the observed data, whose errors are comparable to, or smaller than the size of the dots. B/T and n_B for each fitting are shown in the top-right corner of the panel.

Figure 5 compares between the normalized χ^2 (divided by the number of of valid pixels) from the "$r^{1/4} + \exp$" and "$r^{1/n} + \exp$" model fittings in the r-band. We can see that the χ^2 from "$r^{1/4} + \exp$" model are systematically larger than that from "$r^{1/n} + \exp$" model, although the difference is small. This again indicates that "$r^{1/n} + \exp$" model is superior to "$r^{1/4} + \exp$" model for describing the light profiles of early-type galaxies. To see how the fittings with two models would affect the measured B/T ratio, we show the difference between the two model values of B/T as a function of n_B in Figure 6.
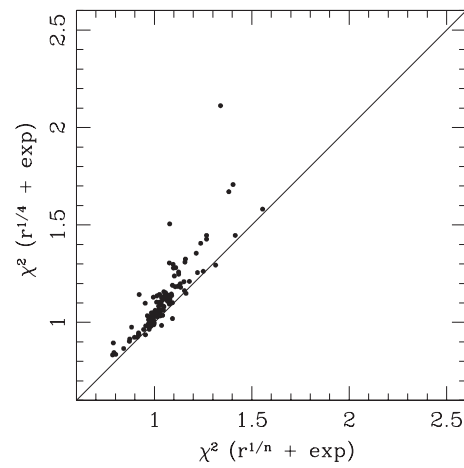
Fig. 5 Comparison between the normalized χ^2 of fittings ($r-$band) with the "$r^{1/4}$ + exp" and "$r^{1/n}$ + exp" models for 129 sample galaxies.

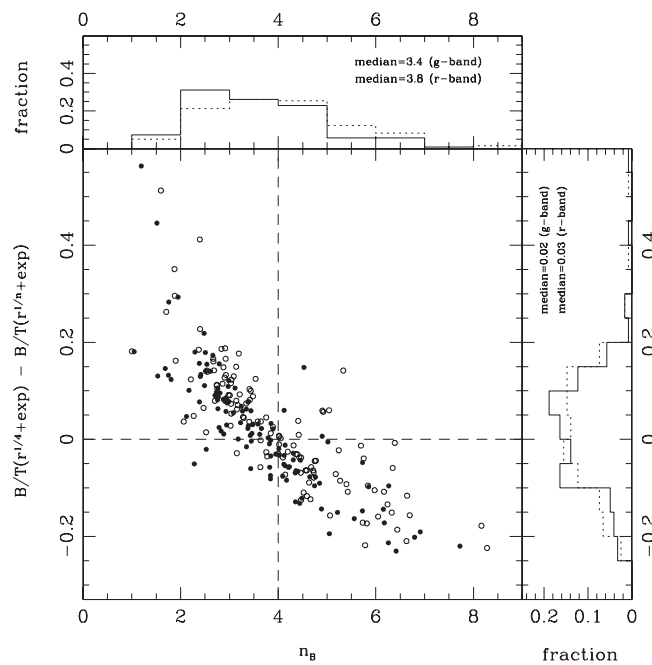**Fig. 6** Difference between the "$r^{1/4}$ + exp" and "$r^{1/n}$ + exp" model fittings of B/T as a function of n_B in the g-band (filled circles) and in the r-band (open circles). The two marginal fractional distributions are shown by the histograms across the top and on the right (solid lines for the g-band and dotted lines for the r-band.)

We can see that the larger the deviation of bulge profile from de Vaucouleurs profile ($n = 4$), the larger the difference in B/T is. A systematic trend can be seen here: the "$r^{1/4}$ + exp" model fitting tends to over-estimate the B/T values of galaxies with $n_B < 4$, and under-estimate those of galaxies with $n_B > 4$.

All the fittings in both the g- and r-bands not only can produce converged parameter sets, but almost all the reduced χ^2 are less than 2 and the majority are around 1, which indicates that our fitting procedure is proper.

Seven of the sample galaxies have $r_{e,B}$ less than the FWHM of seeing, $B/T > 0.95$, or $h < 1.5$ FWHM of seeing in one or both bands. In these cases the derived components would not be reliable because the disk has sizes as small as the seeing, and too small a fraction of the light.

3.3 Fourier Expansion

It has been found that isophotal shapes of early-type galaxies correlate with many of their important characteristics (Bender et al. 1988,1989; Faber et al. 1997; Rest et al. 2001; Hao et al. 2006). It is meaningful to compare the 2-D bulge/disk light decomposition with the isophotal shapes. Accordingly, we also performed an isopthotal shape analysis of our sample galaxies. The isophotal shapes of the sample galaxies are measured using the IRAF task ELLIPSE (Jedrzejewski 1987), in which an ellipse is drawn from the best fitting isophote. The intensity along the ellipse is then expanded in Fourier series,

$$I(\theta) = I_0 + \sum (A_n \cos n\theta + B_n \sin n\theta), \tag{1}$$

where I_0 is the intensity averaged over the ellipse, and A_n and B_n are the higher order Fourier coefficients. If an isophote is a perfect ellipse, then all the coefficients, $(A_n, B_n), (n = 1, \cdots, \infty)$, will be exactly zero. Bender et al. (1988) adopted the following approach. The isophote is described by a function $R(\theta)$ where $R(\theta)$ are the polar coordinates centered at the center of the best fitted ellipse. The deviation of an isophote from a perfect ellipse can be expanded with Fourier series in the polar angle,

$$\delta R(\theta) = R(\theta) - R_{\rm el}(\theta) = a_0 + \sum (a_n \cos n\theta + b_n \sin n\theta), \tag{2}$$

where $R_{\rm el}(\theta)$ denotes the best-fitted ellipse, and a_0 the average deviation averaged over the polar angle. The first five coefficients (a_0, a_1, b_1, a_2 and b_2) are zero within the errors as they are found from fitting. The lowest order significant deviations from zero are a_3, b_3, a_4, b_4, etc. It is found that the most significant non-zero component of the Fourier expansion is the a_4 parameter (corresponding to the $\cos 4\theta$ term). By the sign of this parameter E/S0 galaxies were classified into disky ($a_4 > 0$) and boxy ($a_4 < 0$) galaxies. The *ellipse* outputs A_n, divided by the semi-major axis length (a) and the local gradient, which gives a_n/a parameters, as used by Bender et al. (1988). So our analysis can be directly compared with the previous studies (e.g., Bender et al. 1988,1989; Hao et al. 2006). We carried out photometry with the same elliptical isophotes in both g- and r-bands, which are obtained from $r-$band images as shown in Figure 3. Because a_4/a usually changes along the radius, the value on a special position may not reflect the characteristics of the overall deviations from the ellipse. We thus use the quantity ($\langle a_4/a \rangle$) which is intensity-weighted mean of a_4/a between 2 times FWHM of a realistic PSF and where the local surface brightness $\mu = 25$ mag arcsec^{-2} in the g-band to describe the isophotal shape (e.g., Jørgensen & Franx 1994; Hao et al. 2006). The standard deviation of $\langle a_4/a \rangle$ is calculated according to the formula of error propagation, and that of other retrieved parameters in this paper are also calculated in the same way.

4 RESULTS AND ANALYSIS

4.1 Correlations between Parameters

Correlations of structural parameters from 2-D bulge/disk light decomposition in a single band have been found to be consistent with the results obtained by de Jong et al. (2004). In view of this, we made the decomposition in both the g- and r-bands, so we can compare the structural parameters obtained from the two bands.

Figure 7 shows the results with the "$r^{1/n} + \exp$" model fitting. We can see that most of the structural parameters obtained from the two colors are consistent with each other except that B/T and n_B are, on average, larger in the r-band than in the g-band. This is because the color of the bulge is a little redder than the color of the disk in some sample galaxies. This noted, we will give only the results from one band. Figure 8 plots the bulge-to-total light ratio (B/T) versus the bulge Sérsic index n_B in the g-band. We find these two parameters to be positively correlated. A Spearman rank-order (S-R) correlation analysis gives a
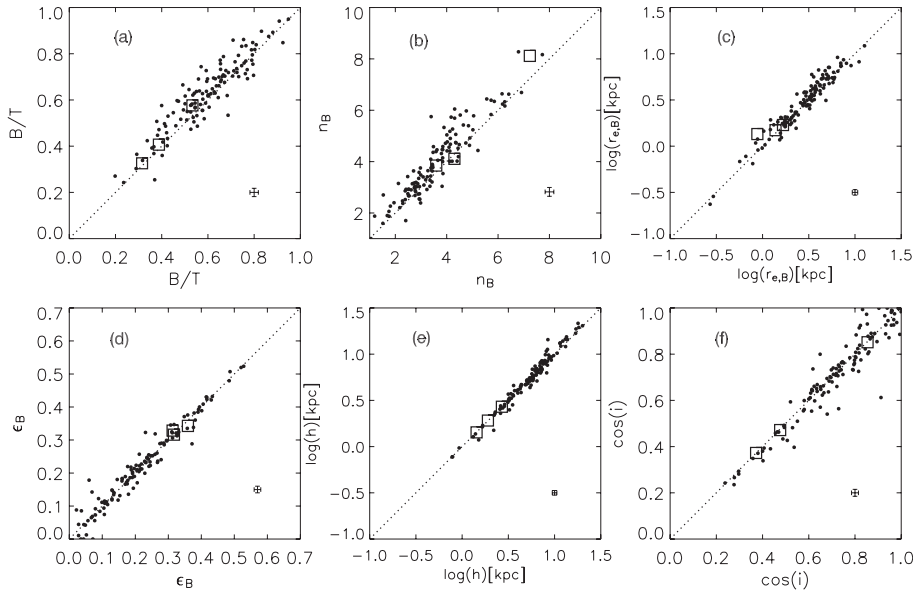
Fig. 7 Comparison of parameters fitted by the "$r^{1/n} + \exp$" model in the g-band (on the x-axis) and the r-band (y-axis) for 122 sample galaxies. The parameters are (a) Bulge-to-total light ratio B/T; (b) Bulge Sérsic index n_B; (c) Effective radius of bulge $r_{e,B}$; (d) Ellipticity of the bulge ϵ_B; (e) Scale length of the disk h; (f) Cosine of the inclination angle of the disk $\cos(i)$. The line of equality is shown as a dotted line in each panel. Three galaxies from SAURON (NGC 3156, NGC 4270 and NGC 5831) are shown with open squares. Crosses mark the typical errors.
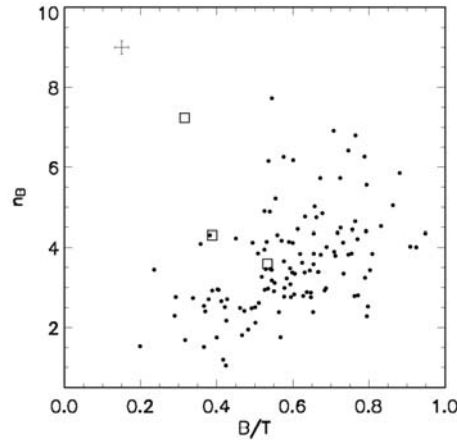
Fig. 8 Bulge-to-total light ratio (B/T) versus bulge Sérsic index n_B in the g-band. Spearman rank-order correlation analysis gives a correlation coefficient of 0.51 at a very high significance level ($P = 2.66 \times 10^{-9}$). Three SAURON galaxies (NGC 3156, NGC 4270 and NGC 5831) are shown with open squares.

correlation coefficient of 0.51 at a very high significance level ($P = 2.66 \times 10^{-9}$). This result means that as the bulge fraction increases, the Sérsic index also gets larger statistically.

In Figure 9 we show a plot of the bulge size versus the disk scale from the "$r^{1/n} + \exp$" (red dots) and "$r^{1/4} + \exp$" (blue dots) model fittings, respectively. S-R correlation analysis gives a correlation coefficient of 0.75 (0.61) and a significance level $P = 1.05 \times 10^{-23}$ ($P = 5.03 \times 10^{-14}$) for the "$r^{1/n} + \exp$" ("$r^{1/4} +$
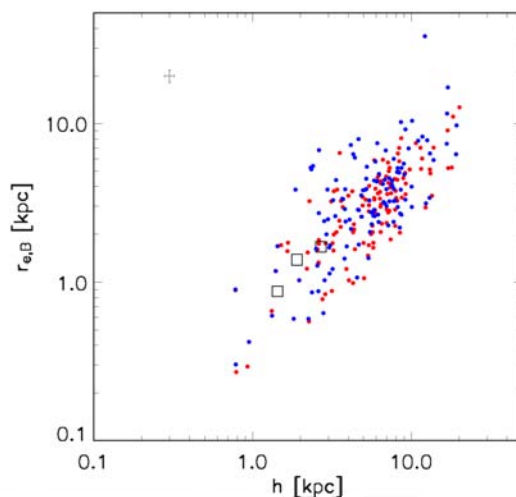
Fig. 9 Disk scale length h versus bulge semi-major axis effective radius $r_{e,B}$ in the g-band from fittings with the "$r^{1/n} + \exp$" (red dots) and "$r^{1/4} + \exp$" (blue dots) models respectively. Spearman rank-order (S-R) correlation analysis gives a correlation coefficient of 0.75 (0.61) at a very high significance level of $P = 1.05 \times 10^{-23}$ ($P = 5.03 \times 10^{-14}$) for the "$r^{1/n} + \exp$" ("$r^{1/4} + \exp$") fitting. Three SAURON galaxies (NGC 3156, NGC 4270 and NGC 5831) are shown with open squares.

exp") model fitting. It shows that they are strongly correlated. This correlation was already presented by Iodice et al. (1999) and de Jong et al. (2004), but here it is much more obvious in our analysis, possibly because of better photometry here. It was suggested that this correlation may imply a possible bulge-disk coupling during galaxy formation and evolution or that angular momentum may have played an important role (Idoice et al. 1999).

Figure 10 shows a plot of isophotal shape parameter $\langle a_4/a \rangle$ vs. B/T for the two fitting models. Standard S-R correlation gives a correlation coefficient of 0.09 (0.08) and a significance level of 0.35(0.36) for the "$r^{1/n} + \exp$" ("$r^{1/4} + \exp$") model. It means that there is no correlation between isophotal shape and B/T. Our analysis also has shown that there is no significant correlation between $\langle a_4/a \rangle$ and n_B either, which is understandable because there is a correlation between n_B and B/T.

4.2 Color Properties

A tight correlation between color and luminosity in early-type galaxies called the color-magnitude relation (CMR), has been known from early researches on these galaxies (Larson, Tinsley & Caldwell 1980; Visvanathan & Sandage 1997; Terlevich et al. 1999; Cool et al. 2006). Later research found that a CMR holds not only for early-type galaxies but may exist for disk galaxies (Tully, Mould & Aronson 1982; Chang et al. 2006). The origin of the CMR is a hotly debated topic, even though it has been thought to be universal. We compare the CMRs for whole galaxies and detected components from the 2-D light decomposition. In Figure 11, panel (a) shows the CMR of whole galaxies from the observations (black symbols) and from model fitting with "$r^{1/n} + \exp$" (red symbols). Panel (b) comapres the fittings from the "$r^{1/n} + \exp$" model (red symbols) and the "$r^{1/4} + \exp$" model (blue symbols). We measure the corresponding parameters with the same isophote in the two bands down to the g-band local surface brightness $\mu = 25\,\text{mag arcsec}^{-2}$. The same way is used for the calculation with the models. The results show that the "$r^{1/n} + \exp$" model and the observations give almost the same tight CMR, with a scatter of only ~ 0.03, but the "$r^{1/4} + \exp$" model gives a slightly bigger scatter (~ 0.05). This implies that our fitting has properly recovered the color parameters of whole galaxies.

The CMRs of the detected bulge and disk components are shown in panels (c) and (d), respectively. It shows that the bulges and disks of early-type galaxies also follow a similar CMR as the whole galaxies, but
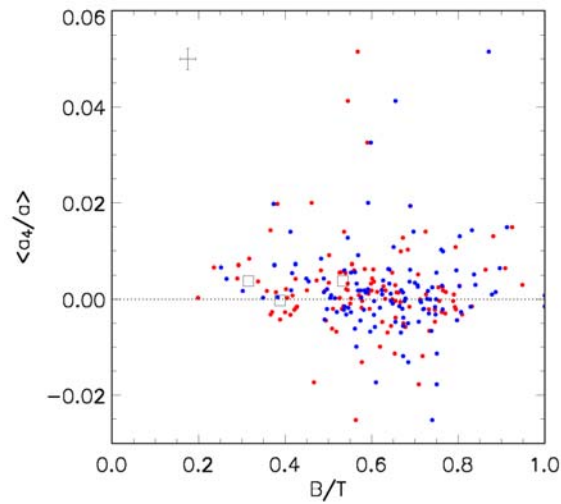
Fig. 10 Bulge-to-total light ratio (B/T) versus isophotal shape parameter $\langle a_4/a \rangle$ in the $g-$band from the "$r^{1/n} + \exp$" (red dots) and "$r^{1/4} + \exp$" (blue dots) model fittings respectively. A Spearman rank-order correlation analysis shows no significant correlation between B/T and $\langle a_4/a \rangle$ for both fitting models. Three SAURON galaxies (NGC 3156, NGC 4270 and NGC 5831) are shown with open squares.
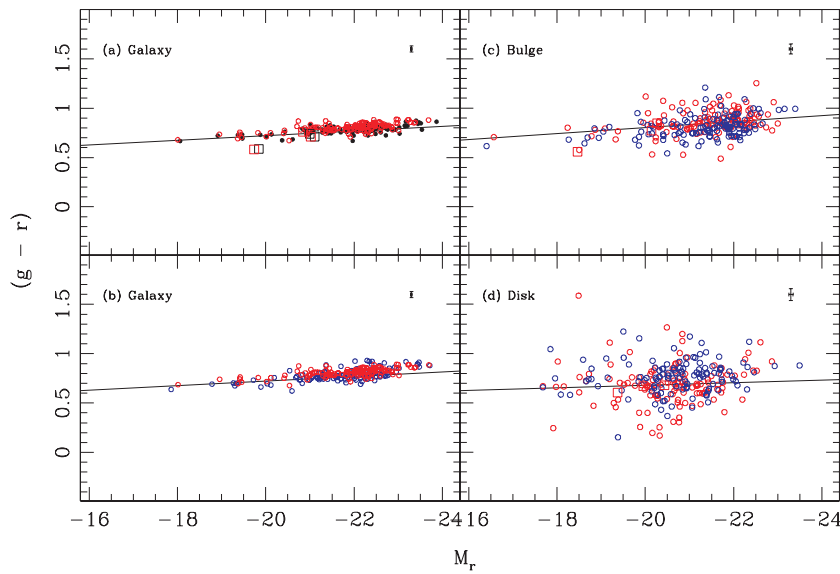

Fig. 11 Color-Magnitude Relation (CMR) of 122 sample galaxies, and their bulges and disks. (a) (g-r) color of whole galaxy vs. r-band absolute magnitude $M_{r,T}$. The filled circles denote the observed data, the open circles, the model results. The solid line is the best-fit line for the observed data. (b) g-r color of whole galaxy vs. r absolute magnitude $M_{r,T}$ for the two models. The solid line is the best linear fit to the observed data. (c) Bulge g-r color vs. r-band absolute magnitude $M_{r,B}$. The solid line is the best linear fit for data from the "$r^{1/n} + \exp$" model; (d) Disk g-r color vs. r-band absolute magnitude $M_{r,D}$. The solid line is the best linear fit for data from the "$r^{1/n} + \exp$" model; Red signs are for the "$r^{1/n} + \exp$" model fitting, and blue signs are for the "$r^{1/4} + \exp$" model fitting. The median error bars are shown in the right-top corner of each panel. Three SAURON galaxies (NGC 3156, NGC 4270 and NGC 5831) are shown by squares.

with a scatter of ~ 0.1 magnitude for the bulges and ~ 0.2 magnitude for the disks. Both "$r^{1/4} + \exp$" and "$r^{1/n} + \exp$" fittings gave nearly the same scatters for the bulges and the disks. The larger scatters here may be caused by the larger errors in their magnitudes inferred from the decomposition in each color and amplified when we combine them into one color. Moreover, galaxy profiles in two different colors usually have some slight differences due to the existence of color gradients. A key step in reducing the scatter is to know how to do the decomposition in the two bands in a consistent way. We can see that the detected bulges and disks in early-type galaxies have nearly the same g-r color, apart from a small difference. This implies that they may have nearly the same stellar population. This result is consistent with McDermid et al. (2006) who stated that the larger stellar disks embedded in early-type galaxies have a stellar population with no distinct differences from the spheroids of galaxies.

4.3 The Fundamental Plane

Early-type galaxies are found to obey a tight relation among their physical properties. This relation can be expressed as a plane in a 3-dimensional parameter space defined by central velocity dispersion σ_0, equivalent effective surface brightness I_0 and equivalent effective radius R_0 (Dressler et al. 1987; Djorgovski & Davis 1987). Relations among these quantities have been found to be of the form,

$$R_0 = C\sigma_0{}^A I_0{}^B, \tag{3}$$

power exponents A and B and coefficient C. The plane defined by the relation has been named the Fundamental Plane (FP). Bender, Burstein & Faber (1992) introduced a different expression for the FP in terms of a κ space, by a simple orthogonal transformation,

$$\begin{aligned}
\kappa_1 &= \lg(R_0\,\sigma_0^2)/\sqrt{2}, \\
\kappa_2 &= \lg(I_0^2\sigma_0^2/R_0)/\sqrt{6}, \\
\kappa_3 &= \lg(I_0^{-1}\sigma_0^2/R_0)/\sqrt{3}.
\end{aligned} \tag{4}$$

They proved that the new κ coordinate system turns out to be more meaningful physically. For example, κ_1 is proportional to the logarithm of the mass, and κ_3 is proportional to the logarithm of the mass-to-light ratio. The projection on ($\kappa_1 - \kappa_2$) plane corresponds to a face-on view of FP, and the projections on ($\kappa_1 - \kappa_3$) and ($\kappa_2 - \kappa_3$) planes correspond to two edge-on projections. The new coordinate system has been used often in subsequent studies of the FP of early-type galaxies (e.g., Burstein et al. 1997; Bernardi et al. 2003b). It is well known that the FP has an intrinsic scatter, whose origin remains unclear. Simple models predict that the presence of disks in E/S0 galaxies can introduce the scatter since E and S0 galaxies are mixed by visual classification. However, there has been no distinct observational evidence for this. Here, we address the question whether or not the distribution of early-type galaxies on the FP depends on the bulge-to-total ratio (B/T). To this end, we divide our sample into two parts according as $B/T > 0.7$ or ≤ 0.7 in g-band. Then, we compare their distributions on the FP in the κ space.

In the previous works, the equivalent effective radius R_0 and other parameters of galaxies were derived from a fit of the classical de Vaucouleurs $R^{1/4}$-law profile to the aperture photometry (e.g.,Jørgensen, Franx & Kjærgaard 1995; Reda et al. 2005). Recently, some authors (e.g. Cappellari et al. 2006) used the improved Sérsic profiles to determine these quantities, and argued that the quantities obtained with different methods differ substantially in some cases. In this work, we perform 2-D elliptical fitting on each sample galaxy with a Sérsic profile model, and determine its semi-major axis effective radius Re_T and ellipticity ϵ_T. The equivalent effective radius R_0 of the galaxy is then calculated by $R_0 = Re_T\sqrt{1 - \epsilon_T}$. The mean equivalent surface brightness $\langle SB_e \rangle$ is obtained by the isophote enclosing half of the light of total galaxy. According to Bernardi et al. (2003a), the central velocity dispersion σ_0 can be corrected into a standard relative circular aperture defined as one-eighth of the equivalent half-light radius R_0 by:

$$\frac{\sigma_{\mathrm{cor}}}{\sigma_0} = \left(\frac{R_{\mathrm{fiber}}}{R_0/8}\right)^{0.04}, \tag{5}$$

where $R_{\mathrm{fiber}} = 1.5$ arcsec for SDSS and R_0 is the equivalent effective radius of the galaxy measured in arcsecond. Thus, an FP in κ space can be set up following Equation (6), in which $\lg(I_0)$ is defined to
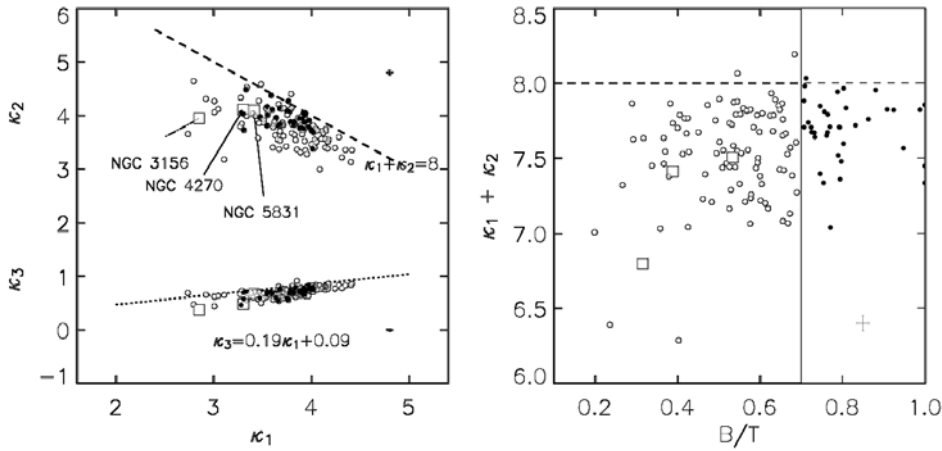
Fig. 12 Distributions on the FP of 129 sample galaxies in g-band viewed in the κ space projections. In left panel galaxies are split into two groups by B/T in the g-band: Those with $B/T > 0.7$ denoted by filled circles and $B/T \leq 0.7$ denoted by open circles. The dashed line is $\kappa_1 + \kappa_2 = 8$ (marking the "zone of avoidance"). The dotted line shows the best linear fit on the ($\kappa_1 - \kappa_3$) projection of the FP obtained by Bernardi et al. (2003b). The relation of B/T versus $\kappa_1 + \kappa_2$ for the two groups of galaxies is shown in the right panel. The dashed line denotes the same as in the left panel. The solid line shows $B/T = 0.7$. The standard S-R correlation analysis gives a correlation coefficient of 0.27 at a high significance level ($P = 1.9 \times 10^{-3}$). Three SAURON galaxies (NGC 3156, NGC 4270 and NGC 5831) are marked by open squares. Median error bars are shown in each panel.

be $0.4 \times (27 - \langle SB_e \rangle)$ (Bender, Burstein & Faber 1992; Bernardi et al. 2003b). The FP in ($\kappa_1 - \kappa_2$) and ($\kappa_1 - \kappa_3$) projections obtained from the g-band data of the sample galaxies is shown in the left panel of Figure 12. The dotted line is the best fit on the ($\kappa_1 - \kappa_3$) projection of the FP obtained with a larger and relatively complete sample of early-type galaxies by Bernardi et al. (2003b). The dashed line on the top is the line of $\kappa_1 + \kappa_2 = 8$, which marks what is termed the "zone of avoidance" by Burstein et al. (1997). It can be seen that galaxies with larger B/T ratios are distributed tighter and closer to the line marking the "zone of avoidance" than those with smaller B/T ratios. This means early-type galaxies with relatively large disk fractions have larger scatters on the FP. We also show the relation of $\kappa_1 + \kappa_2$ versus B/T in the right panel of Figure 12. Here, the dashed line marks again the "zone of avoidance" and the scatter from the projection of the ($\kappa_1 + \kappa_2$) is shown. We can see the correlation between $\kappa_1 + \kappa_2$ and B/T. The standard S-R correlation analysis gives a correlation coefficient of 0.27 at a significance level ($P = 1.9 \times 10^{-3}$). It is found that early-type galaxies with relatively large bulge-to-total light ratios tend to lie closer to the "zone of avoidance" on the FP in κ space, and sources with larger disks components lie, on average, farther away from the "zone of avoidance". This fact seems to indicate that the presence of disks in early-type galaxies is one of the factors to cause the scatter in the FP.

A test of the dependence of distribution on the observed g-r color is shown in Figure 13. For the comparison we divide the sample galaxies into two groups according to their g-r colors: a redder group with colors redder than the median color of 0.785 mag and a bluer group comprising the others. The redder group is denoted by filled circles and the bluer group, open circles. We can see clearly that the redder galaxies tend to concentrate in the region of larger κ_1, while the bluer galaxies have an opposite trend. It is understood that κ_1 is proportional to the logarithm of the mass of the galaxies, and κ_3 is proportional to the logarithm of the mass-to-light ratio. We find that the values of κ_3 are confined to a very narrow range, that is, the mass-to-light ratio spans a relatively narrow range. If all early-type galaxies have approximately the same mass-to-light ratio, then κ_1 is proportional to the logarithm of the luminosity of the galaxy. According to the well-known CMR of early-type galaxies, the brighter galaxies are redder. Therefore, the redder galaxies will tend to be distributed in the region of large κ_1 on the FP. We also give the relation of $\kappa_1 + \kappa_2$ vs. the observed g-r color in the right panel of Figure 13. An S-R correlation analysis shows they are positively
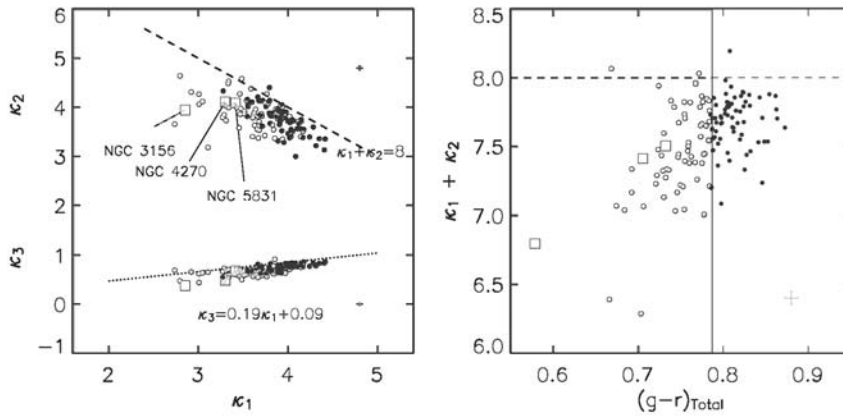
Fig. 13 Distribution on the FP of 129 sample galaxies in the g-band viewed in the κ space projection. Galaxies are split into two groups by the observed g-r color: filled circles for galaxies with g-$r_{Total} > 0.785$, open circles for those with g-$r_{Total} \leq 0.785$. Their g-r_{Total} versus $\kappa_1 + \kappa_2$ plots are shown in the right panel. The standard S-R correlation analysis gives a correlation coefficient of 0.43 at a high significance level ($P = 2.2 \times 10^{-7}$). The solid line shows g-$r_{Total} = 0.785$. The dashed line or the dotted line in each panel denotes the same as in Fig. 12. The three SAURON galaxies (NGC 3156, NGC 4270 and NGC 5831) are marked with open squares. Median error bars are shown in each panel.
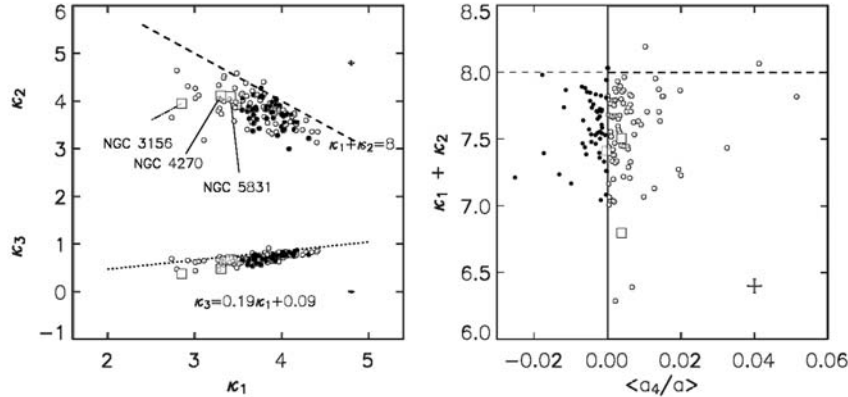

Fig. 14 Distribution on FP of 129 sample galaxies in $g-$band viewed in the κ space projection. In the left panel, the galaxies are split into two groups by isophotal shape parameter $\langle a_4/a \rangle$: Those with $\langle a_4/a \rangle > 0$ (disky) are denoted by open circles and those with $\langle a_4/a \rangle < 0$ (boxy), by filled circles. The $\langle a_4/a \rangle$ versus $\kappa_1 + \kappa_2$ plots for the two classes of galaxies are shown in the right panel. Standard S-R correlation analysis gives a correlation coefficient of only 0.04 at a very low significance level ($P = 0.62$) The solid line is $\langle a_4/a \rangle = 0$. The dashed line or the dotted line in each panel are the same as in Fig. 12. Three SAURON galaxies (NGC 3156, NGC 4270 and NGC 5831) are marked with open squares. Median error bars are shown in each panel.

correlated with a correlation coefficient of 0.43 at a very high significance level ($P = 2.2 \times 10^{-7}$). It is shown that the redder early-type galaxies tend to lie closer to the "zone of avoidance" on the FP in κ space. We have investigated the dependence of the distribution on the FP on the isophotal shapes of the galaxies. Usually objects with intensity-weighted isophotal shape parameter $\langle a_4/a \rangle < 0$ are called boxy and those with $\langle a_4/a \rangle > 0$, disky. In Figure 14, the boxy and disky objects are denoted with filled and open circles respectively. The relation of $\kappa_1 + \kappa_2$ vs. $\langle a_4/a \rangle$ is shown in the right panel of Figure 14. A standard S-R correlation analysis shows that there is no significant correlation.

4.4 Comparisons with SAURON

We have shown that the bulge and disk components obtained from 2-D light decomposition have some global statistical properties. However, without kinematical observations, we cannot confirm whether all the detected bulges and disks are good representatives of their kind. As a piece of supplementary work, we cross-identified the 48 early-type galaxies observed by SAURON with SDSS DR2. There are nine objects (NGC 2768, NGC 3156, NGC 4270, NGC 5308, NGC 5813, NGC 5831, NGC 5838, NGC 5845 and NGC 5846) brighter than magnitude 13.5 in Sloan r-band. Two of them, NGC 5813 and NGC 5838, are located at the edge of the frames. NGC 5846 has strong contamination by companion objects. NGC 2768 has a distinct dusty feature (Emsellem et al. 2004), and NGC 5308 is an edge-on S0 galaxy and has a significant dust lane. Therefore, there are four objects (NGC 3156, NGC 4270, NGC 5831 and NGC 5845) left that satisfy the selection criteria of our sample. Two-dimensional light decomposition of these four sources was made. Not all the sources have spectral information in SDSS. We found and corrected their redshifts from NASA/IPAC Extragalactic Database (NED) for the Local Group infall, following Blanton et al. (2005), but we neglected the correction for peculiar velocities since they are only on order of $200 - 300\,\text{km s}^{-1}$ (Blanton et al. 2005). Their velocity dispersions were taken from the Lyon/Meudon Extragalactic Database (LEDA, see Paturel et al. 1997) and aperture correction was done in the same way as we did for the sample galaxies. Results obtained are as follows.

By the 2-D decomposition, NGC 3156 has $B/T = 0.31$ with $h/r_{e,B} = 1.63$ in the g-band. From the SAURON observations, NGC 3156 has a comparable outer rotating component (Emsellem et al. 2004).

By our decomposition, NGC 4270 hss $B/T = 0.39$ with $h/r_{e,B} = 1.61$ in the g-band. The SAURON observations resolved it to have a distinct rotating component at large radius.

By our decomposition, NGC 5831 has $B/T = 0.53$ and with $h/r_{e,B} = 1.38$ in the g-band. Peletier et al. (1990) have revealed an underlying disk component. The SAURON observations revealed it to have only a slowly rotating component at large radius. Emsellem et al. (2004) pointed out that the SAURON maps need to be re-binned to reach the required signal-to-noise ratio, but the velocity field in NGC 5831 has been reported with kinematically isolated structures (Davies et al. 1983; Peletier et al. 1990).

NGC 5845 has been observed by HST to harbor an edge-on, thin central disk. The SAURON observations also indicate the presence of a central rotating component, and the OASIS observation has shown a beautifully resolved disk component (Richard et al. 2006). Our decomposition almost failed to reveal this faint disk ($B/T = 0.99$ in the g-band and 0.94 in the r-band), which may be due to this nuclear disk being removed by the masking of the central region in our decomposition. To check this we repeated the decomposition with no-masked images. We found that it has a small disk light fraction ($B/T = 0.84$ in the g-band and 0.87 in the r-band) and a small disk scale length ($h = 1.98\,\text{arcsec}$ in g and $1.96\,\text{arcsec}$ in r). After comparison with the SAURON results, we can see that a rotationally supported component has been detected, which corresponds to a disk component detected by our 2-D decomposition. The data obtained from three of those four SAURON sources have been shown in Figures 6 –14 with open squares. Because the decomposition of NGC 5845 is heavily affected by masking, we did not include it on the figures. We can see from these figures that all three sources follow the same relations as the other sample galaxies. The SAURON results provide us with evidence that our 2-D decomposition is a reasonable good tool for the statistical analysis of bulge and disk components of early-type galaxies.

5 SUMMARY AND DISCUSSION

We use the publicly available code GIM2D (Simard et al. 2002) to perform 2-D bulge/disk light decomposition on an approximately magnitude-limited sample of local, early-type galaxies. The decomposition was made in both the g- and the r-bands, with data based on more careful photometry with better sky background subtraction and realistic PSFs. In the decomposition, the bulge component is modelled with a Sérsic profile or de Vaucouleurs ($n = 4$) profile, and the disk component, with an exponential profile. The structural parameters in both the g- and r-bands were determined by fitting the g- and r-band photometric data separately. We emphasize that the disk component derived by our decomposition is mainly the outer disk since the center region with size of the seeing was masked in our fitting. We also use the ELLIPSE of IRAF (Jedrzejewski 1987) to perform Fourier expansion on sample galaxies to determine their intensity-weighted isophotal shape parameters $\langle a_4/a \rangle$. The fitted parameters for all sample galaxies are available online (*http://www.chjaa.org/2008/2008_8_5p503*).

We have made comparisons between the bulges and disks obtained from our decomposition with the SAURON observations, and the result give support to our belief that the bulges and disks found by our decomposition could be fair representatives of their kind. We have found that the bulge-to-total light ratio (B/T) and the bulge Sérsic index n_B are positively correlated, which means that early-type galaxies with larger Sérsic index n_B are more bulge-dominated ones. Also the bulge and disk scale sizes of early-type galaxies are well correlated, which could imply a possible coupling between the bulge and the disk during their formation and evolution. The same trend has been found by Iodice et al. (1999) and de Jong et al. (2004), but we still do not have an explanation for this correlation. Our results show that there is no correlation in either the B/T vs $\langle a_4/a \rangle$ plot or in the n_B vs $\langle a_4/a \rangle$ plot. This indicates that a galaxy's isophotes may not be determined by its bulge fraction.

Our decompositions in both the r- and g-bands enabled us to analyze properties connected with the colors of the bulges and disks. We find that both the bulges and the disks resulting from our decomposition satisfy the well-known colr-magnitude relation, though with somehow larger dispersions. The later may be caused by the uncertainty in the decomposition in the two colors (Section 3.2), which is about $5\% - 15\%$ and $20\% - 30\%$ in the derived parameters for the disks and the bulges, respectively. The bulge and disk components have almost the same g-r color, which implies that the bulges and disks of early-type galaxies are composed of nearly the same stellar population.

We investigated the behavior of early-type galaxies of different B/T ratios on the Fundamental Plane. Early-type galaxies with larger B/T ratios appear to follow a tighter relation than those with smaller B/T ratios, and also tend to lie closer to the so-called "zone of avoidance" (Burstein et al. 1997). It is shown that the positions of early-type galaxies on the FP in κ space depend on the color of the galaxies: The redder galaxies dominate the region of larger κ_1 on the FP and lie closer to the "zone of avoidance". These results imply the disk components (likely supported by rotation) can cause the scatter on the FP, and age/metallicity may also affect the position of early-type galaxies on the FP, if color is an indicator of age and/or metallicity. We find there is no evident difference in the scatter on the FP in κ space between disky and boxy galaxies. This supports our results given above that the disky isophotes may not connect closely with the existence of a significant disk component in the galaxy.

We notice that even though the GIM2D can be used to decompose early-type galaxies into bulge and disk components quantitatively, there are several factors which may cause the decomposition to have considerable errors. As we have seen, the central nuclear disks can not be reliably separated due to effect of seeing and/or in some cases they may not be possible to be fitted with a simple bulge plus disk model. Besides, as pointed out by de Jong et al. (2004) and Tasca & White (2005), a real disk can not be an infinite thin one, as the model assumes. As we know most luminous elliptical galaxies have stellar haloes. In the two-component decomposition the light from the halo is most likely taken as bulge and/or disk. Therefore, GIM2D can only be used for the statistical analysis of a large sample. One should be cautious when one uses it to investigate properties of an individual galaxy.

References

Abazajian K., Adelman-McCarthy J. K., Agüeros M. A. et al., 2004, AJ, 128, 502

Allen P. D., Driver S. P., Graham A. W. et al., 2006, MNRAS, 371, 2

Bacon R., Copin Y., Monnet G. et al., 2001, MNRAS, 326, 23

Balcells M., Quinn P. J., 1990, ApJ, 361, 381

Bender R., Doebereiner S., Moellenhoff C., 1988, A&AS, 74, 385

Bender R., Surma P., Doebereiner S. et al., 1989, A&A, 217, 35

Bender R., Burstein D., Faber S. M., 1992, ApJ, 399, 462

Bernardi M., Sheth R. K., Annis J. et al., 2003a, AJ, 125, 1817

Bernardi M., Sheth R. K., Annis J. et al., 2003b, AJ, 125, 1866

Bertin E., Arnouts S., 1996, A&AS, 117, 393

Binney J., Merrifield M. 1998, In: Galactic Astronomy, Princeton University Press, Princeton, New Jersey, 186

Blanton M. R., Schlegel D. J., Strauss M. A. et al., 2005, AJ, 129, 2562

Burstein D., Bender R., Faber S., Nolthenius R., 1997, AJ, 114, 1365

Burstein D., Saglia R. P., Colless M., Davies R. L., McMahan R. K., Wegner G., 2001, in ASP Conf. Ser. 230, Galaxy
 Disks and Disk Galaxies, ed.J.G. Funes and E.M. Corsini (San Francisco: ASP), 153

Caon N., Capaccioli M., D'Onofrioo M., 1993, MNRAS, 265, 1013

Capaccioli M. 1987, In: The Structure and Dynamics of Elliptical Galaxies, ed. T. de Zeeuw(Dordrecht;kluwer), 47

Capaccioli M. 1989, In: Corwin H. G., Bottinelli L., eds, The World of Galaxies, Springer-Verlag, Berlin, p.208

Cappellari M., Bacon R., Bureau M. et al., 2006, MNRAS, 366, 1126

Carter D., 1987, ApJ, 312, 514

Chang R. X., Shen S. Y., Hou J. L., Shu C. G., Shao Z. Y., 2006, MNRAS, 372, 199

Cool R. J., Eisenstein D. J., Johnston D. et al., 2006, AJ, 131, 736

Davies R. L., Efstathiou G., Fall S. M., Illingworth G., Schechter, P. L., 1983, ApJ, 266, 41

Davies R. L. 2000, In: Encyclopedia of Astronomy and Astrophysics, Ed. by Paul Murdin, article 1672

de Jong R. S., Simard L., Davies R. L. et al., 2004, MNRAS, 355, 1155

Djorgovski S., Davis M., 1987, ApJ, 313, 59

Dressler A., 1987, ApJ, 317, 1

de Vaucouleurs G., 1948, Ann. Astrophys, 11, 247

Emsellem E., Cappellari M., Peletier R. F. et al., 2004, MNRAS, 352, 721

Faber S. M., Tremaine S., Ajhar E. A. et al., 1997, AJ, 114, 1771

Fried D. L., 1996, J. Opt. Soc. Am., 56, 1372

Graham A., Colless M., 1997, MNRAS, 287, 221

Hao C. N., Mao S., Deng Z. G., Xia X. Y., Wu H., 2006, MNRAS, 370, 1339

Hernquist L., Barnes J. E., 1991, Nature, 354, 210

Hubble E., 1936, The Realm of the Nebulae (New Haven: Yale Univ. Press), 36

Iodice E., D'Onofrioo M., Capaccioli M., 1999, ASP Conf. Ser., 176, 402

Jedrzejewski R. I., 1987, MNRAS, 226, 747

Jørgensen I., Franx M., 1994, ApJ, 433, 553

Jørgensen I., Franx M., Kjærgaard P., 1995, MNRAS, 273, 1097

Jørgensen I., Franx M., Kjærgaard P., 1996, MNRAS, 280, 167

Kent S. M., 1985, ApJS, 59, 115

Kormendy J., 1984, ApJ, 287, 577

Larson R. B., Tinsley B. M., Caldwell C. N., 1980, ApJ, 237, 692

Lauer T. R., 1985, MNRAS, 216, 429

Lugger P. M., 1984, ApJ, 278, 51

Marleau F. R., Simard L., 1998, ApJ, 507, 585

Metropolis N., Rosenbluth A., Rosenbluth M., Teller A., Teller E., 1953, Journal of Chemical Physics, 21, 1087

Michard R., 2002, A&A, 384, 763

Peletier R. F., Davies R. L., Illingworth G. D., Davies L. E., Cawson M., 1990, AJ, 100, 1091

Paturel G., Andernach H., Bottinelli L. et al., 1997, A&AS, 124, 109

Reda F. M., Forbes D. A., Hau G. K. T., 2005, MNRAS, 360, 693

Rest A., van den Bosch F. C., Jaffe W. et al., 2001, AJ, 121, 2431

McDermid R. M., Emsellem E., Shapiro K. L. et al., 2006, MNRAS, 373, 906

Rix H.-W., White S. D. M., 1990, ApJ, 362, 52

Saglia R. P., Burstein D., Baggley G. et al., 1997, MNRAS, 292, 499

Saha P., Williams T. B., 1994, AJ, 107, 1295

Sérsic J. L., 1968, Atlas de Galaxies Australes (Cordoba: Observatories Astronomica)

Simard L., Willmer C. N. A., Vogt N. P. et al., 2002, ApJS, 142, 1

Stoughton C., Lupton R. H., Bernardi M. et al., 2002, AJ, 123, 485

Tasca L. A. M., White S. D. M., 2005, (astro-ph/0507249)

Terlevich A. I., Kuntschner H., Bower R. G., Caldwell N., Sharples R. M., 1999, MNRAS, 310, 445

Trujillo I., Aguerri J. A. L., Cepa J., Gutiérrez C. M., 2001, MNRAS, 321, 269

Tully R. B., Mould J. R., Aaronson M., 1982, ApJ, 257, 527

Visvanathan N., Sandage A., 1997, ApJ, 216, 214

Weil M. L., Hernquist L., 1993, ApJ, 405, 142

Woolf N. J., 1982, ARA&A, 20, 367

Wu H., Shao Z. Y., Mo H. J., Xia X. Y., Deng Z. G., 2005, ApJ, 622, 244

Young C. K., Currie M. J., 2001, A&A, 369, 736